# Tin-Chelated Trisphosphineoxide Scorpionate Rare-Earth Porphyrinate Complexes: Synthesis and Photophysical Properties

Da Jin,[#] Cedric Uhlmann,[#] Erik K. Schneider, Tim Seifert, Dominik Graf, Sergei Lebedkin, Patrick Weis, Manfred M. Kappes, and Peter W. Roesky*

**ABSTRACT:** A series of seven-coordinated monoporphyrinate rare-earth(III) complexes featuring a novel tripodal tin-chelated trisphosphineoxide scorpionate ligand with the general formula [(TPP)Ln($PPh_2O$)$_3$Sn] (Ln = Y, La, Dy, Er, Ho, Yb; TPP = 5,10,15,20-tetraphenylporphyrinate) were synthesized by reactions of the potassium tripodal scorpionate ligand [Sn($PPh_2O$)$_3$K] with porphyrinate rare-earth metal chlorides [(TPP)LnCl(dme)] (Ln = Y, Dy, Er, Ho, Yb) or porphyrinate lanthanum borohydride [(TPP)La$BH_4$(thf)$_2$]. The complexes were characterized by single-crystal X-ray diffraction, NMR spectroscopy, and ion mobility mass spectrometry. All complexes emit weak red TPP-based fluorescence, accompanied by near-infrared emission of Er, Ho (rather weak), and Yb (relatively intense with a quantum yield of 1% in dichloromethane solution) of the corresponding complexes. Despite the low intensity, the red fluorescence is characteristic (as referred to the parent free-base TPP) and can be used together with optical absorption for analytical evaluation. Similar photophysical properties can be expected for monoporphyrinate rare-earth metal complexes of other tripodal ligands with a similar binding to the (TPP)Ln moiety.

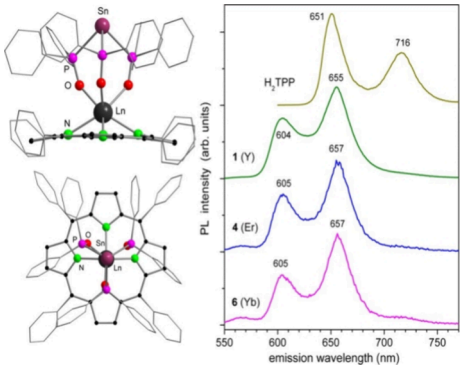


## INTRODUCTION

The luminescent properties of the trivalent lanthanides are unique and remain in focus of intensive applied and basic research. Their sharp emissive f-f transitions cover a wide spectral range from the ultraviolet (~200−400 nm, including emission bands of $Ce^{III}$ and $Gd^{III}$), to visible (e.g., of $Eu^{III}$ and $Tb^{III}$) and near-infrared (NIR, e.g., of $Yb^{III}$, $Er^{III}$ and $Nd^{III}$).[1,2] The NIR luminescence deserves since recently a particular attention, as it has potential applications in biological imaging and telecommunications.[3] Due to the parity-forbidden character of f-f transitions, an efficient excitation of $Ln^{III}$ cations requires energy transfer from a chromophore,[4] which serves as an antenna for light absorption. Accordingly, the ligands in Ln complexes have to fulfill not only a chemical, but also an important photophysical function. Porphyrin derivatives have proven to be efficient antenna ligands.[5−7] They absorb both in the UV and visible range and bind strongly to almost all $Ln^{III}$ cations due to their nitrogen sites. Moreover, their excited singlet or triplet states may well sensitize $Ln^{III}$ NIR emitters.[3]

Besides this, porphyrins exhibit a highly delocalized $\pi$-system and their metal complexes can be incorporated into different condensed-phase environments, such as metal−organic frameworks[8,9] and liquid crystals.[10,11] In concentrated solutions, porphyrins can form aggregates with the size and arrangement depending on various parameters, including concentration and pH value.[12−14] Recently, several porphyrin complexes with transition metals have also been studied in gas phase by ion mobility, photoelectron, and photodissociation spectroscopy.[15−21] Furthermore, porphyrin lanthanide complexes have been probed for magnetic dipolar sensors,[22] tumor diagnosis[23] and single-molecule magnets (SMMs).[24,25] Regarding different plausible structures of porphyrin lanthanide complexes, monoporphyrinate ones appear especially interesting, as they can allow further modification and functionalization via a supplementary ligand (which is necessary to complete capping and stabilization of a $Ln^{III}$ cation). However, such complexes remain rare,[26−29] in part due to the challenges posed by typical high-temperature reaction conditions, which often result in the formation of undesired double- and triple-decker side products.[30,31] Specifically, most monoporphyrinate complexes were derived so far from Kläui's tripodal ligand, [($\eta^5$-$C_5H_5$)Co{$PO(OR)_2$}$_3$]$^-$ (Figure 1A).[24,32−35] Additionally, several other monoporphyrinate complexes coordinated by the hydridotris(pyrazol-1-yl)borate ligand (Figure 1B) were synthesized.[28,36,37]

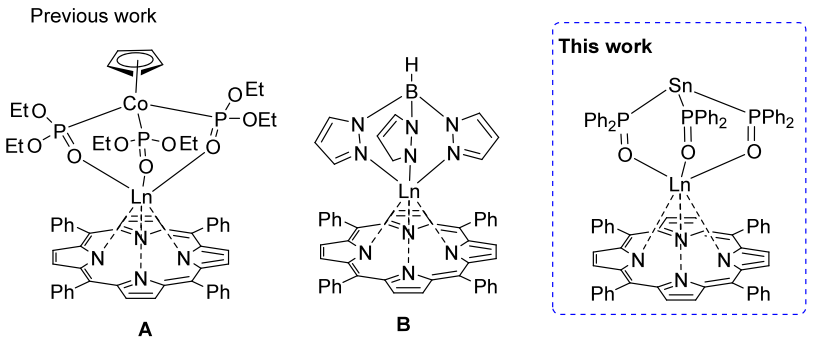


**Figure 1.** Two typical examples of monoporphyrinate lanthanide complexes functionalized by tripodal ligands (A and B)[24,28] and compounds synthesized in this work.[46,47]

Moreover, phosphine oxide ligands, particularly those with $Ph_2P{=}O$ moieties, are widely utilized in the synthesis of rare-earth complexes.[38−42] The highly polar P=O bond, often represented as a double bond, is thought to possess a significant ionic character.[43,44] This makes the oxygen atom highly electron-rich and capable of forming stable electrostatic interactions with positively charged lanthanide ions. While ligands containing one or two $Ph_2P{=}O$ groups have been extensively developed, those with three or more $Ph_2P{=}O$ groups are limited due to steric demands and solubility challenges.[45]

In this report, we present the synthesis and characterization of a new series of stable monotetrapheneylporphyrinate complexes of La, Dy, Er, Ho, Yb and Y coordinated by a novel anionic tripodal scorpionate tin ligand $[Sn(PPh_2O)_3]^-$.[46,47] They were investigated in the solid state, solution and in gas phase (from ion mobility measurements). Furthermore, photophysical properties of the complexes were determined, primarily at ambient temperature.

## RESULTS AND DISCUSSION

A salt elimination reaction between three equivalents of potassium diphenylphosphinoxide $[KOPPh_2]$[48] and $SnCl_2$ led to the isolation of the Sn tripodal ligand $[\kappa^3\text{-}Sn(P(O)Ph_2)_3K]$ ($L^{Sn}K$) (Scheme 1).

**Scheme 1. Synthesis of the Sn Tripodal Ligand $[L^{Sn}K]$**

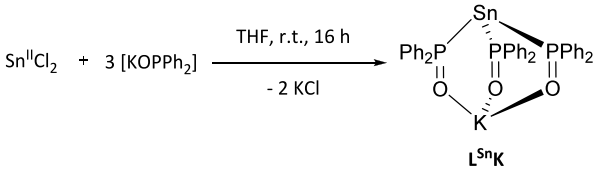


In the solid state, complex $[L^{Sn}K]$ is present as a dimeric $[\{\kappa^3\text{-}Sn(P(O)Ph_2)_3K\}_2]$ structure, which is bridged by the coordination of the O2 and O2' atoms to K and K' (Figure 2). Complex $[L^{Sn}K]$ corresponds to a tripodal ligand, which has three oxygen donor sites. The P−O bond lengths are between 1.473(3) Å and 1.504(3) Å and thus in the range of P=O double bonds.[49] The Sn−P distances are between 2.5806(11) Å and 2.6544(12) Å and the K−O bond lengths are in the range between 2.504(3) Å and 2.688(3) Å.

NMR spectroscopic studies were carried out in THF-$d_8$. Three signals with intensities 2:1:2 at $\delta$ 7.48, 7.19, and 7.00 ppm are observed in the $^1$H NMR spectrum. These could be assigned to the phenyl protons in the corresponding ortho, meta and para positions to the phosphorus atom. In the $^{31}P\{^1H\}$ NMR spectrum, a signal is observed at $\delta$ 54.7 ppm with corresponding satellites due to the coupling with two tin isotopes $^{117}$Sn and $^{119}$Sn.[50] The $^{119}Sn\{^1H\}$ NMR spectrum is split into a quartet at $\delta$ 209.6 ppm due to coupling with the neighboring phosphorus atoms, with a $^1J_{PSn}$ coupling constant of 1621 Hz. The new ligand $\{L^{Sn}\}^-$ resembles Kläui's tripodal ligand, $[(\eta^5\text{-}C_5H_5)Co\{PO(OR)_2\}_3]^-$.[51−53] Both feature three P=O coordination sites, which act as chelating ligands and form a kind of metalla-phospha bicyclo[2.2.2]octane cage.

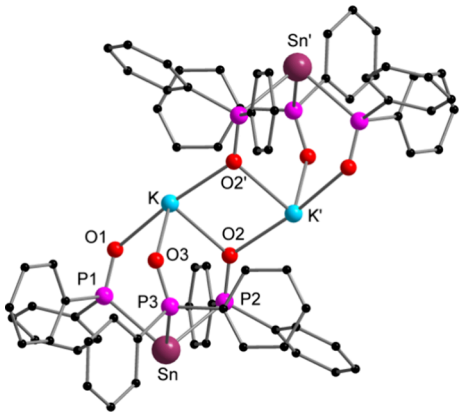


**Figure 2.** Molecular structure of the complex $[\kappa^3\text{-}Sn(P(O)Ph_2)_3K]$ ($L^{Sn}K$) in the solid state. Hydrogen atoms are omitted for clarity. Selected bond lengths [Å] and angles [°]: Sn−P1 2.6544(12), Sn−P2 2.5806(11), Sn−P3 2.6373(12), P1−O1 1.473(3), P2−O2 1.482(3), P3−O3 1.504(3), K−O1 2.504(3), K−O2 2.688(3), K−O3 2.651(3), K−O2' 2.563(3), P1−Sn−P2 91.50(3), P1−Sn−P3 85.94(4), P2−Sn−P3 95.12(4), O1−K−O2 86.20(9), O1−K−O3 83.95(9), O2−K−O3 89.58(9).[47]

For synthesizing mixed $\{L^{Sn}\}$/TPP rare-earth complexes, the monoporphyrinate lanthanum species $[(TPP)LaBH_4(thf)_2]$ was prepared first by reacting $[Li_2TPP(dme)_3]$[54] with $[La(BH_4)_3(thf)_3]$.[55,56] Its structure was confirmed by X-ray diffraction analysis (Figure S18). Subsequently, by refluxing a mixture of $[L^{Sn}K]$ and $[(TPP)LaBH_4(thf)_2]$ or the previously reported compounds $[(TPP)LnCl(dme)]$ (Ln = Y, Dy, Ho, Er, Yb) in THF, monoporphyrinate rare-earth metal complexes of the general formula of $[(TPP)Ln(PPh_2O)_3Sn]$ (Ln = Y (**1**), La (**2**), Dy (**3**), Er (**4**), Ho (**5**), Yb (**6**)) were obtained as dark red crystals with moderate yields (40−55%) (Scheme 2).

Single crystals suitable for X-ray diffraction analysis were obtained by slow diffusion of *n*-pentane into the corresponding dichloromethane (DCM) solutions. All complexes exhibit similar structural features in general. They all crystallize in the

**Scheme 2. Synthesis of Monoporphyrinato Rare-Earth Complexes with the Sn Tripodal Ligand**

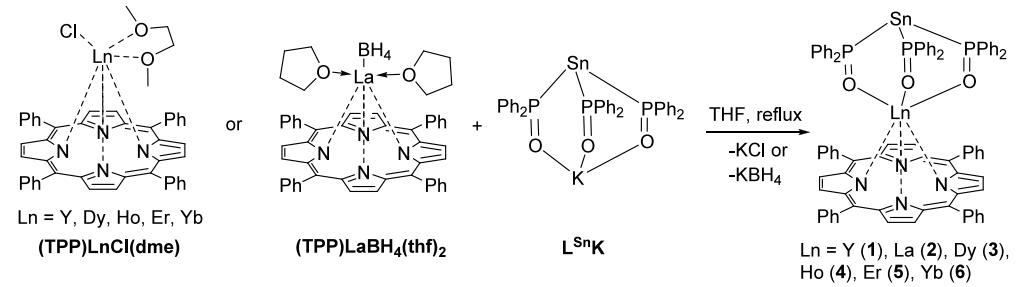


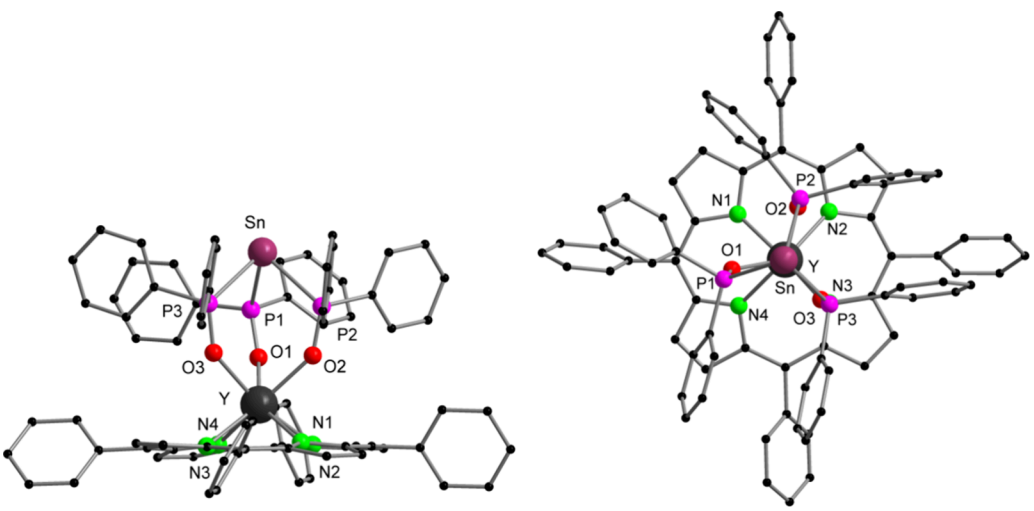


**Figure 3.** Molecular structure of **1** in the solid state: side view (left) and top view (right). All hydrogen atoms are omitted for clarity. Selected bond lengths (Å) (see for the Table 1 and Figures S20–S24 for the isostructural complexes **2**–**6**): Sn–P1 2.6221(11), Sn–P2 2.6100(10), Sn–P3 2.6167(11), P1–O1 1.524(3), P2–O2 1.521(3), P3–O3 1.528(3), Y–O1 2.287(3), Y–O2 2.300(3), Y–O3 2.283(3), Y–N1 2.379(3), Y–N2 2.392(3), Y–N3 2.396(3), Y–N4 2.390(3).[46,47]

**Table 1. Selected Structural Data for $[(Tpp)Ln(PPh_2O)_3Sn]$ Complexes**[a]

| $(TPP)Ln(PPh_2O)_3Sn$ | M–N (av) | M–O (av) | M–Sn | M–$N_{plane}$[b] | M–$O_{plane}$[b] | M–$P_{plane}$[b] |
|---|---|---|---|---|---|---|
| Y | 2.3893(3) | 2.290(3) | 4.6583(4) | 1.2148(3) | 1.5097(3) | 2.9967(3) |
| La | 2.5132(5) | 2.431(4) | 4.7175(1) | 1.4115(5) | 1.6066(4) | 3.1018(4) |
| Dy | 2.3980(3) | 2.3097(3) | 4.6699(1) | 1.2276(3) | 1.5245(3) | 3.0107(3) |
| Ho | 2.3870(4) | 2.2960(4) | 4.6644(1) | 1.2106(4) | 1.5158(4) | 3.0034(4) |
| Er | 2.3783(4) | 2.2857(4) | 4.6412(1) | 1.1951(1) | 1.5027(1) | 2.9850(1) |
| Yb | 2.3598(6) | 2.2727(6) | 4.6508(0) | 1.1699(6) | 1.4977(6) | 2.9804(6) |

[a]All measurements in angstroms (Å). [b]Distance from the rare-earth metal atom to the plane defined by the N/O/P atoms.

orthorhombic space group $Pna2_1$ with two cocrystallized DCM molecules in their asymmetric units. Here only the molecular structure of the Y compound is shown in Figure 3 and cocrystallized solvent molecules have been omitted for clarity. In complex **1**, the bond distances between the coordinated O atoms and the Y ion are nearly equivalent, ranging from 2.283(3) to 2.300(3) Å, comparable to those reported $Ph_2P{=}O$ supported Y complexes.[38,42,57] The three mean planes ($N_4$, $O_3$ and $P_3$) are nearly parallel, with dihedral angles of 3.21°, 0.50°, and 3.46° between the $N_4$ and $O_3$ planes, $O_3$ and $P_3$ planes, and $N_4$ and $P_3$ planes, respectively. For better comparison, selected structural data of all complexes are presented in Table 1.

Due to the large ionic radii of the rare-earth metals, the metal ions do not fit into the cavity of the porphyrin ring. Instead, they are located above the plane defined by the four nitrogen atoms of the porphyrin. The remaining Sn tripod ligands compensate for the residual positive charge and complete the coordination sphere of the metal ions. As a result, the metal centers adopt a distorted capped octahedral geometry, consistent with the distortion parameters calculated using the SHAPE 2.1 program (Table S3, with the La complex as an example).[58] Specifically, the capped octahedron is composed of three of the four porphyrin N atoms and three ligating O atoms of the Sn tripod, with the final porphyrin N atom forming the capping group. Table 1 presents the metal–ligand distances, which differ based on the size of the metal ions. As the ionic radii of the metal ions increase, the distances between the metal and ligand atoms become more elongated. The porphyrin ring adopts a domed conformation due to the metal ion's inability to fit into its cavity. This conformation maximizes the interactions between the rare-earth metal ions and the porphyrin nitrogen atoms.

Due to the highly paramagnetic nature of Yb, Er, Ho, and Dy metal ions present in the complexes, NMR spectra with sharp and well-defined signals were only obtained for complexes **1** (Y) and **2** (La). The NMR spectra were recorded in $CDCl_3$. Proton peak assignments are determined by integration along with $^1H-^1H$ correlation spectroscopy (COSY). For complex **1**, the singlet signal at $\delta$ 8.88 ppm is assigned to the $\beta$-position proton on the pyrrole, while the signals at $\delta$ 8.15 to 7.55 ppm are assigned to the phenyl groups in the porphyrin moiety (Figure S5). The $\beta$-position proton is comparable to that in $[Y(TPP)(cyclen)Cl]^+$ (8.86 ppm).[59] The protons on the phenyl group of the Sn tripod appear from $\delta$ 6.88 ppm to 5.97 ppm. In the $^{13}C\{^1H\}$ NMR spectrum, the resonances of $\alpha$ and $\beta$-carbons of the porphyrin moiety appear at 123.2 and 150.8 ppm, respectively, which were identified by $^{13}C$ DEPT-135 NMR spectroscopy and 2D $^1H-^{13}C$ HMBC analysis. The NMR spectra of complex **2** have shown similar characteristics as complex **1**.

**Mass Spectra, Collision Induced Dissociation and Ion Mobility Measurements.** Complexes **1-6** were characterized by electrospray ionization high-resolution mass spectrometry (ESI-HR-MS) in negative mode as chlorine adducts, see Figures S32–S37. A CID (collision induced dissociation) study of $[(TPP)Y(PPh_2O)_3SnCl]^-$ (Figure S38) found two dominant fragmentation channels: $[(TPP)Y(PPh_2O)_3SnCl]^- \rightarrow [(TPP)Y(PPh_2O)_2]^- + [(PPh_2O)SnCl]$ and $[(TPP)Y(PPh_2O)_3SnCl]^- \rightarrow [(TPP)Y(PPh_2O)] + [(PPh_2O)_2SnCl]^-$ in line with the expected bond stability. Gas phase ion mobility measurements of $[(TPP)Ln(PPh_2O)_3SnCl]^-$, (Ln = Y, Dy, Ho, Er, Yb) yielded mobilograms consisting of one narrow Gaussian shaped peak and collision cross sections that agree within the experimental resolution (Figure S39). This clearly indicate that in all cases the same geometrical structure of the ions was observed in the gas phase—in line with the very close structures of these compounds found in the crystalline state (see above).

**Photophysical Properties.** The absorption spectra of **1-6** in the visible range are contributed by the TPP moiety and are very similar, as expected regarding the closely related structures of these lanthanide complexes. The spectra are shown exemplarily for DCM solutions of **1**, **2** and **4** in Figure 4 and for other compounds in Figure S25. Referring to the parent free-base tetraphenyl porphyrin ($H_2TPP$) dissolved in DCM, the sharp and intense Soret band (SB) due to the allowed $S_0 \rightarrow S_2$ transition[60] red-shifts from 417 nm to ca. 429 nm in **1-6** (Figure 4). The extinction coefficient of $4.7 \times 10^5$ $M^{-1}cm^{-1}$ measured at the SB maximum in $H_2TPP$ remains nearly the same in **1**, **2** ($4.6 \times 10^5$ $M^{-1}cm^{-1}$) and moderately increases to $(5.1-5.4) \times 10^5$ $M^{-1}cm^{-1}$ in **3-6** (Table S4), correlating with some narrowing of the SB in the latter compounds. In the Q-band region between ~490 and 680 nm, corresponding to the symmetry forbidden $S_0 \rightarrow S_1$ transition,[60] a characteristic vibronic pattern with four components is observed for $H_2TPP$, whereas **1-6** show two major components at ca. 560 and 600 nm attributed to the Q(0,1) and Q(0,0) transitions. The absorption spectra of **1-6** resemble those of other metalloporphyrins,[61] and, not surprisingly, practically coincide with the spectra of Ln porphyrinate complexes with Kläui's tripodal ligand or its derivatives,[24,28,32–34] which possess the same TPP-Ln-$O_3$ binding pattern as in **1-6**. It is perhaps worthwhile to note that different TPP complexation/functionalization patterns can also result in a blue shift of the SB (as referred to $H_2TPP$), for instance, in the cofacially linked tris-porphyrin and its metal complexes (with the SB peak at 404–406 nm).[62]

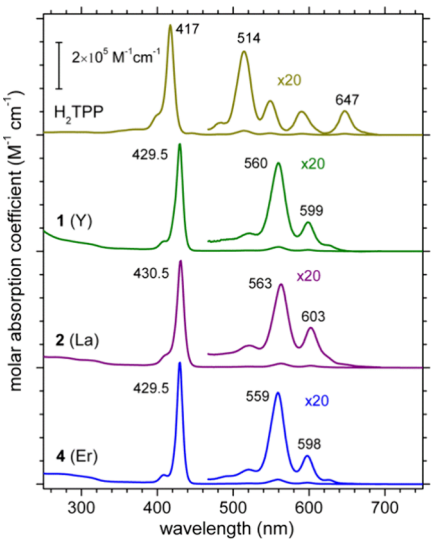


**Figure 4.** Absorption spectra of $[(TPP)Ln(PPh_2O)_3Sn]$ complexes **1** (Y), **2** (La) and **4** (Er) in comparison with $H_2TPP$, measured in dichloromethane at room temperature.

Regarding photoluminescence (PL) properties of Ln complexes **1-6**, we found that they emit in solution a similar weak red fluorescence arising from the TPP moiety, which mirrors the Q-band absorption. Figure 5 compares the spectra

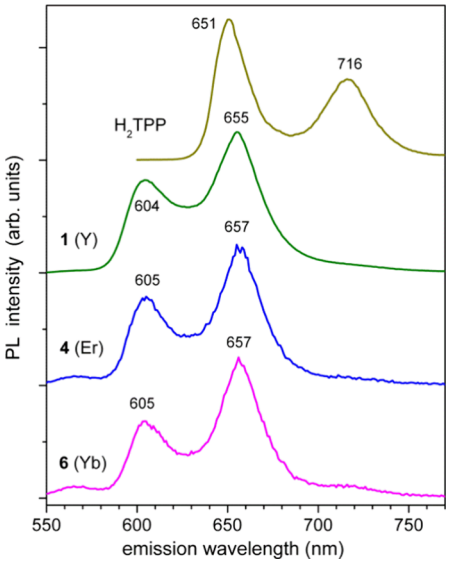


**Figure 5.** Fluorescence emission (PL) spectra of $H_2TPP$ and $[(TPP)Ln(PPh_2O)_3Sn]$ complexes **1**, **4** and **6** (Ln = Y, Er, Yb) in dichloromethane at room temperature. The emission was excited at 417 and 430 nm for $H_2TPP$ and the Ln complexes, respectively.

of this emission exemplary for **1**, **4** and **6** with the fluorescence of $H_2TPP$ in DCM at room temperature. The excitation spectra follow well the SB and Q-band absorption profile as illustrated for **1** in Figure S26. $H_2TPP$ emits two characteristic bands at 651 and 716 nm (Q(0,0) and Q(1,0) transitions), whereas **1-6** emit related bands at ca. 605 and 657 nm. Accordingly, the Stokes shift between the maxima of the Q(0,0) subbands in absorption and emission amounts to about

100 and 150−200 $cm^{-1}$ in $H_2TPP$ and **1**-**6**, respectively. Again, we note that the emission of **1**-**6** closely resembles that of other metalloporphyrins, also mirroring with a small Stokes shift two Q bands in absorption.[63,64] The fluorescence quantum yield, $\Phi_{FL}$, is quite low, which is typical for porphyrin complexes with rare earth metals.[28,65,66] The $\Phi_{FL}$ values of $6 \times 10^{-3}$ and on the order of $10^{-4}$ were determined for **1** (Y) and **3**-**6** (Dy, Er, Ho, Yb), respectively, upon excitation into the Soret band (Table S4) - in comparison to $\Phi_{FL}$ = 0.09 for $H_2TPP$. The low efficiency is accompanied by subnanosecond short fluorescence lifetimes (Figure S27, Table S4), as referred to $\tau_{FL}$ = 8.8 ns for $H_2TPP$ in DCM (at $\lambda_{exc}$ = 403 nm, see the SI).

The weak fluorescence of the above complexes can be attributed to electronic coupling in the metal-TPP system, generating effective channels of nonradiative decay.[65] Somewhat intriguing, however, are the different effects on the TPP fluorescence efficiency and lifetime (as referred to $H_2TPP$, see Table S4): whereas $\Phi_{FL}$ decreases dramatically by a factor of 600−2500 in **3**-**6**, a decrease in $\tau_{FL}$ - both measured at Soret band ($S_2$) excitation wavelengths - depends on the lanthanide and is moderate (by a factor of 7−20) in **3**, **5** and **6**. In contrast, the reduction of $\Phi_{FL}$ to $6 \times 10^{-3}$ in the yttrium complex **1** correlates well with $\tau_{FL}$ = 0.5 ns (Table S4). A possible explanation might be that the lanthanides in **3**-**6** can also strongly affect and contribute deactivation of the initially populated $S_2$ excited state of TPP. We plan to investigate this issue in more detail, by extending the fast PL decay setup to excitation sources also covering the Q-band ($S_1$ state) spectral range.

Fast intersystem crossing (ISC) to the triplet excited state $T_1$ is considered as a major deactivation channel of the TPP singlet excited states in (metallo)porphyrins.[63,64] A related phosphorescence is, however, typically weak and only detectable at low temperatures, e.g., in frozen glassy solutions at 77 K. For complexes with rare earth metals, it has mostly been observed for Y, La, Gd, or Lu *i.e.* for the metals with no open f-shell (Y) or with no f-levels lying below $T_1$.[67,68] In accordance with those observations, TPP phosphorescence could not be detected for **1**-**6** in (argon-purged) DCM at ambient temperature. In frozen DCM at 77 K, however, **1** (Y) shows two additional, weak emission bands at *ca.* 800 and 890 nm (Figure S30), which were assigned to the main TPP phosphorescence band and its vibronic satellite. Analogous bands at ca. 805 and 900 nm, with the intensity comparable to the red fluorescence, were detected for **2** (La) in frozen DCM (not shown). The other lanthanide complexes remained nonphosphorescent at 77 K.

Deactivation of the TPP excited states can also effectively proceed by an energy transfer to low-lying (accepting) f-levels of suitable $Ln^{III}$ cations. This can sensitize a characteristic f-f emission of the latter. In a series of the complexes described here, this relaxation pathway and accompanying near-infrared (NIR) emission are expected for **4** (Er), **5** (Ho) and **6** (Yb). Indeed, the characteristic NIR emission patterns of these lanthanides were recorded in the range of ~900−1700 nm (see experimental details in the SI) with relative intensities in the order: **6** (Yb) ≫ **4** (Er) ≫ **5** (Ho). Figure 6 shows the corresponding spectrum for **6** (Yb) excited at 430 nm in a dichloromethane solution at room temperature. The quantum yield of $Yb^{III}$ emission at around 1000 nm amounts to $\Phi_{PL}$ = 0.01, i.e. it is ~300 times more intense than the TPP-based (intraligand) red fluorescence at ~580−700 nm. Its lifetime was determined as 37 $\mu$s. The NIR emission of $Er^{III}$ in **4** at

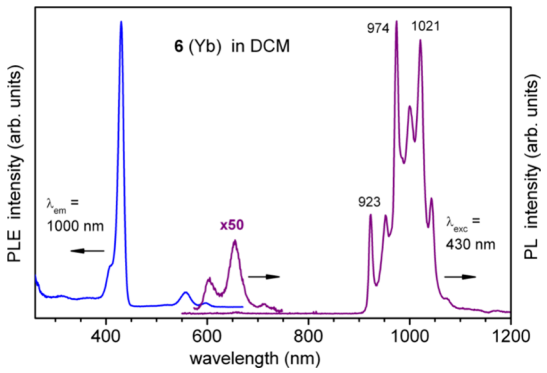


**Figure 6.** Near-infrared emission (PL) of the trivalent Yb in complex **6** dissolved in dichloromethane (~$5 \times 10^{-6}$ M) and excited at 430 nm ($T$ = 295 K). The emission is sensitized by energy transfer from the TPP moiety (as illustrated by the excitation (PLE) spectrum) and its integral intensity is ~300 times higher than that of the TPP-based red fluorescence within 580−700 nm (shown on the same scale as the emission of $Yb^{III}$).

about 1540 nm could also be readily recorded (Figure S29), but of a lower intensity, with $\Phi_{PL}$ estimated as $2 \times 10^{-5}$, i.e. comparable to $\Phi_{FL}$ of the TPP fluorescence in **4**. Even a weaker NIR emission band of $Ho^{III}$ at 1202 nm was detected for complex **5** in DCM (Figure S29, $\Phi_{PL}$ was not quantified). Despite such different NIR emission efficiencies in **4**-**6**, the energy transfer between the TPP antenna and the $Ln^{III}$ cations likely occurs with a high rate in all these complexes, but the further relaxation is to a great extent nonradiative in **4** (Er) and **5** (Ho). The major electronic deactivation pathways introduced by the $Ln^{III}$ cations in the $[(TPP)Ln(PPh_2O)_3Sn]$ compounds, also including yttrium in **1**, are thus nonradiative.

The above PL properties described for **1**-**6** in solution were in general found in the solid samples as well. These include the weak TPP-based red fluorescence at about 650 nm as shown exemplarily for solid (polycrystalline) **1**, **2** and **4** at T = 3 and 295 K in Figure S30. Similar to the solutions, the NIR phosphorescence of the TPP moiety within ~800−950 nm was only observed for solid **1** (Y) and **2** (La). It was the most prominent at low temperatures and particularly for complex **2** (Figure S30). Furthermore, the lanthanide NIR emissions of solid **4**-**6** closely followed in terms of the spectral shape and intensity (Yb ≫ Er ≫ Ho) the corresponding emissions in solution (Figure S31). All emission bands demonstrated a quite moderate temperature dependence between 3 and 295 K. In addition, practically the same quantum yield (0.011) and lifetime (39 $\mu$s) were measured for the $Yb^{III}$ NIR emission of solid **6** (Yb) as compared to the values in solution. These observations suggest a mainly intramolecular character of electronic relaxation in **1**-**6**, with a relatively small influence of the crystalline surrounding.

In line with previous reports on the stability of Ln porphyrinate complexes,[28] we found that **1**-**6** are stable as solids stored under normal conditions in a freezer, but decompose in commercial anhydrous DCM (as well as in dichloroethane and $CCl_4$) on the time scale of days (**1**, **3**-**6**) or even hours (**2**). The faster decomposition of **2** (La) probably correlates with the distinctly larger distances between the La atom and porphyrin ring in this complex (Table 1). Accordingly, freshly prepared solutions of **1**-**6** were used for the above measurements. The decomposition proceeds via demetalation of the porphyrin ligand and formation of the free-

base TPP. It could be readily followed in optical spectra due to the characteristic differences between **1**-**6** and $H_2$TPP, namely, the position of the SB in absorption and Q(0,0), Q(1,0) transitions in fluorescence. For instance, a weak feature at ~720 nm in the fluorescence spectrum of **6** presented in Figure 5 indicates a small admixture of the free-base TPP.

## CONCLUSIONS

We presented a novel tin tripodal ligand $[Sn(PPh_2O)_3]^-$ for a preparation of monoporphyrinate rare-earth metal(III) complexes. A series of such complexes $[(TPP)Ln(PPh_2O)_3Sn]$ (TPP = 5,10,15,20-tetraphenylporphyrinate, Ln = Y, La, Dy, Er, Ho and Yb) were synthesized and characterized by single-crystal XRD, NMR (Ln = Y, La) and ion mobility mass spectrometry (for the anionic $Cl^-$ adducts in gas phase). As it might be expected, the very similar structures were found for the different lanthanides and yttrium in the crystalline state as well as in gas phase. Somewhat more elongated TPP-Ln distances in case of lanthanum correlate with its larger ionic radius. Large similarity is also observed in the photophysical properties of these complexes. Referring to the parent free-base TPP, their absorption and weak red fluorescence spectra, mostly contributed by the TPP moiety, show characteristic shifts of the Soret and Q bands. Near-infrared lanthanide emission was recorded for the complexes of Yb, Er and Ho. The emission of $Yb^{III}$ around 1000 nm is the most effectively sensitized, with *ca.* 1% quantum yield both in dichloromethane solution and in solid state at ambient temperature.

## EXPERIMENTAL SECTION

**General Procedures.** All manipulations of water- and air-sensitive compounds were performed with exclusion of moisture and oxygen in flame-dried Schlenk-type glassware either on a dual manifold Schlenk line, interfaced to a high vacuum ($10^{-3}$ mbar) line or in an argon-filled MBraun glovebox. All solvents were dried by using a MBraun solvent purification system (SPS 800). Tetrahydrofuran was additionally distilled under nitrogen from potassium benzophenone ketyl before storage over 4 Å molecular sieves. $CH_2Cl_2$ was dried by refluxing over $P_2O_5$ and distilled under a nitrogen atmosphere. THF-$d_8$ was dried over Na–K alloy and degassed by freeze–pump–thaw cycles. $CDCl_3$ was distilled over $P_2O_5$ and stored over 4 Å molecular sieves. NMR spectra were recorded on Bruker spectrometers (Avance Neo 300 MHz, Avance Neo 400 MHz or Avance III 400 MHz) at 298 K. Chemical shifts are referenced internally using signals of the residual protio solvent ($^1$H) or the solvent ($^{13}$C{$^1$H}) and are reported relative to tetramethylsilane ($^1$H, $^{13}$C{$^1$H}). The multiplicity of the signals is indicated as s = singlet, d = doublet, dd = doublet of doublets, t = triplet and m = multiplet. Assignments were determined on the basis of unambiguous chemical shifts, coupling patterns and $^{13}$C DEPT experiments or 2D correlations ($^1$H–$^1$H COSY, $^1$H–$^{13}$C HMQC and $^1$H–$^{13}$C HMBC). Elemental analyses were carried out with an Elementar Vario Micro cube from Elementar Analysensysteme GmbH. IR spectra were obtained on a Bruker Tensor 37 spectrometer equipped with a room temperature DLaTGS detector, a diamond ATR (attenuated total reflection) unit and a nitrogen-flushed chamber. In terms of their intensity, the signals were classified into different categories (vs = very strong, s = strong, m = medium, w = weak, and sh = shoulder).

$[Li_2TPP(dme)_3]$,[54] $[La(BH_4)_3(thf)_3]$,[55,56] $[K(OPPh_2)]$[48] and $[TPPLnCl(dme)]$[27] were prepared following literature procedures. Other chemicals are commercially available and used without further purification.

**Synthesis of $[\{\kappa^3$-Sn(P(O)Ph$_2)_3$K$\}_2]$ ($L^{Sn}$K).** A mixture of 5.00 g $[K(OPPh_2)]$ (20.8 mmol, 3.00 equiv) and 1.32 g (6.94 mmol, 1.00 equiv) $SnCl_2$ was suspended in 300 mL THF. After stirring overnight, the mixture was filtered over Celite on a medium porosity sintered glass frit. Afterward all volatiles were removed in vacuo. The residual solid was redissolved in hot toluene. Subsequently the obtained saturated solution was stored at room temperature until the formation of crystalline material was observable. Yield (based on crystals): 4.29 g (5.63 mmol), 81%. $^1$H NMR (400 MHz, THF-$d_8$): $\delta$ [ppm]: 7.48–7.47 (m, 12H, C$H_{Ph}$), 7.21–7.16 (m, 6H, p–C$H_{Ph}$), 7.05–6.95 (m, 12H, C$H_{Ph}$). $^{13}$C{$^1$H} NMR (101 MHz, THF-$d_8$): $\delta$ [ppm]: 144.9 (q), 131.0 (d), 130.5 (t), 129.4 (s), 128.7 (d), 128.4 (m). $^{31}$P{$^1$H} NMR (162 MHz, THF-$d_8$): $\delta$ [ppm]: 54.7 (s). $^{119}$Sn{$^1$H} NMR (149 MHz, THF-$d_8$): $\delta$ [ppm]: −209.6 (q, $^1J_{PSn}$ = 1621 Hz). IR (ATR): $\tilde{\nu}$ (cm$^{-1}$) = 3052 (vw), 2942 (vw), 2858 (vw), 1572 (vw), 1478 (vw), 1433 (w), 1381 (vw), 1304 (vw), 1242 (vw), 1194 (vw), 1128 (m), 1064 (m), 1023 (vw), 996 (vw), 933 (vw), 880 (vw), 848 (vw), 738 (m), 690 (vs), 639 (vw), 613 (vw), 594 (vw), 564 (w), 524 (vs), 487 (s), 460 (w), 424 (vw). Anal. Calcd. for $C_{36}H_{30}KO_3P_3Sn$ (761.36 g/mol): C, 56.79; H, 3.97. Found: C, 56.65; H, 3.73.

**Synthesis of Complexes 1 and 3–5.** THF (10 mL) was added to a mixture of the $[Sn(PPh_2O)_3K]$ (0.152 g, 0.2 mmol) and $[(TPP)LnCl(dme)]$ (Ln = Y, Dy, Er, Ho, Yb) (0.2 mmol) and the resulting mixture was refluxed for 8 h, after which all volatiles were removed under reduced pressure. The resulting solid was extracted with DCM and filtered. Vapor diffusion of *n*-pentane into the DCM solution afforded dark purple single crystals for X-ray diffraction analysis. The mother liquor was removed by cannula and the crystals were dried in vacuo for 1 h affording the title product as a purple solid.

*[(TPP)Y(PPh$_2$O)$_3$Sn] (**1**).* Yield (based on crystals): 0.117 g (0.082 mmol), 41%. $^1$H NMR (400 MHz, $CDCl_3$): $\delta$ (ppm) = 8.88 (s, 8H, *H*-Pyrrole), 8.15 (d, 4H, *J* = 7.3 Hz, Ph (ortho)), 7.77 (d, 4H, *J* = 7.4 Hz, Ph (ortho)), 7.70–7.64 (m, 8H, Ph (meta)), 7.55 (t, 4H, *J* = 7.5 Hz, Ph (para)), 6.88 (t, 6H, *J* = 6.8 Hz, PPh (para)), 6.74 (t, 12H, *J* = 7.0 Hz, PPh (meta)), 5.97 (dd, 12H, *J* = 10.5, 8.0 Hz, PPh (ortho)). $^{13}$C{$^1$H} NMR (101 MHz, $CDCl_3$): $\delta$ (ppm) = 150.8 ($C_{ipso}$-Pyrrole), 144.3 ($C_{ipso}$-Ph or PPh), only one could be detected), 135.1 ($C_{ortho}$-Ph), 134.9 ($C_{ortho}$-Ph), 131.2 (*C*-Pyrrole), 129.7 ($C_{para}$-PPh), 129.2 ($C_{ortho}$-PPh), 127.7 ($C_{meta}$-PPh), 126.8 ($C_{meta}$-Ph), 126.2 ($C_{meta}$-Ph), 125.7 ($C_{para}$-Ph), 123.2 (-C=*C*-C–). IR (ATR): $\tilde{\nu}$ (cm$^{-1}$) = 3049 (w), 1593 (w), 1514 (w), 1476 (m), 1434 (w), 1326 (w), 1197 (w), 1122 (w), 1178 (m), 1109 (sh), 1081 (m), 1064 (m), 1025 (w), 1003 (w), 981 (s), 845 (w), 794 (m), 749 (m), 734 (m), 723 (m), 690 (s), 658 (sh), 620 (w), 576 (w), 526 (vs), 489 (m), 423 (w). Anal. Calcd. for $C_{80}H_{58}N_4O_3P_3SnY$ (1423.91 g/mol): C, 67.48; H, 4.11; N, 3.93. Found: C, 67.35; H, 4.19; N, 4.51.

*[(TPP)Dy(PPh$_2$O)$_3$Sn] (**3**).* Yield (based on crystals): 0.162 g (0.108 mmol), 54%. IR (ATR): $\tilde{\nu}$ (cm$^{-1}$) = 3049 (w), 1593 (w), 1514 (w), 1475 (w), 1434 (m), 1326 (w), 1197 (w), 1120 (s), 1080 (m), 1064 (s), 1025 (w), 1003 (w), 981 (s), 845 (w), 793 (s), 748 (m), 723 (m), 690 (vs), 657 (m), 620 (m), 577 (w), 525 (vs), 488 (s), 422 (w). Anal. Calcd. for $C_{80}H_{58}N_4O_3P_3SnDy$ (1497.50 g/mol): C, 64.17; H, 3.90; N, 3.74. Found: C, 64.06; H, 3.88; N, 3.75.

*[(TPP)Ho(PPh$_2$O)$_3$Sn] (**4**).* Yield (based on crystals): 0.120 g (0.080 mmol), 40%. IR (ATR): $\tilde{\nu}$ (cm$^{-1}$) = 3049 (w), 1592 (w), 1515 (w), 1476 (w), 1434 (m), 1326 (w), 1196 (w), 1176 (w), 1121 (s), 1109 (sh), 1080 (m), 1064 (m), 1025 (w), 1003 (w), 981 (s), 845 (w), 828 (w), 794 (s), 751 (m), 723 (m), 690 (vs), 658 (m), 575 (w), 526 (vs), 489 (m), 472 (m), 423 (w). Anal. Calcd. for $C_{80}H_{58}N_4O_3P_3SnHo$ (1499.93 g/mol): C, 64.06; H, 3.90; N, 3.74. Found: C, 63.69; H, 3.84; N, 3.75.

*[(TPP)Er(PPh$_2$O)$_3$Sn] (**5**).* Yield (based on crystals): 0.132 g (0.088 mmol), 44%. IR (ATR): $\tilde{\nu}$ (cm$^{-1}$) = 3049 (w), 1592 (w), 1515 (w), 1476 (w), 1434 (m), 1326 (w), 1196 (w), 1121 (m), 1109 (sh), 1080 (m), 1064 (s), 1025 (w), 1003 (w), 981 (s), 845 (w), 794 (s), 747 (m), 723 (m), 689 (vs), 657 (m), 620 (w), 577 (w), 524 (vs), 488 (m), 423 (w). Anal. Calcd. for $C_{80}H_{58}N_4O_3P_3SnEr$ (1502.26 g/mol): C, 63.96; H, 3.89; N, 3.73. Found: C, 63.73; H, 3.86; N, 4.39.

*[(TPP)Yb(PPh$_2$O)$_3$Sn] (**6**).* Yield (based on crystals): 0.142 g (0.094 mmol), 47%. IR (ATR): $\tilde{\nu}$ (cm$^{-1}$) = 3050 (w), 1593 (w), 1517 (w), 1478 (w), 1434 (m), 1327 (w), 1197 (w), 1122 (s), 1109 (sh), 1081 (m), 1064 (m), 1025 (w), 1003 (w), 982 (s), 845 (w), 794 (s), 734 (m), 689 (vs), 658 (m), 620 (m), 577 (w), 525 (vs), 489 (m), 424

(w). Anal. Calcd. for $C_{80}H_{58}N_4O_3P_3SnYb$ (1508.05 g/mol): C, 63.72; H, 3.88; N, 3.72. Found: C, 63.82; H, 3.84; N, 3.75.

**Synthesis of Complex [TPPLa(BH$_4$)(thf)$_2$].** THF (20 mL) was added to a mixture of the $[Li_2TPP(dme)_3]$ (0.200 g, 0.223 mmol) and $[La(BH_4)_3(thf)_3]$ (0.089 g, 0.223 mmol). The resulting mixture was stirred overnight and subsequently filtered. Single crystals for X-ray diffraction analysis were obtained by concentrating the THF solution. After crystallization, the complex $[TPPLa(BH_4)(thf)_2]$ exhibited reduced solubility in THF and proved to be unstable in DCM, preventing the recording of suitable NMR spectra. Yield (based on crystals): 0.114 g (0.125 mmol), 56%. IR (ATR): $\tilde{\nu}$ (cm$^{-1}$) = 3095 (w), 3005 (w), 2890 (w), 2397 (w), 2210 (w), 1593 (w), 1575 (sh), 1512 (w), 1470 (w), 1436 (m), 1322 (m), 1237 (w), 1196 (w), 1174 (w), 1149 (m), 1093 (sh), 1067 (m), 1028 (m), 1003 (m), 980 (vs), 917 (w), 872 (m), 793 (vs), 748 (s), 721 (s), 699 (vs), 656 (m), 622 (m), 576 (m), 517 (w), 419 (m). Anal. Calcd. for $C_{52}H_{48}N_4O_2BLa$ (910.70 g/mol): C, 68.58; H, 5.31; N, 6.15. Found: C, 69.20; H, 5.74; N, 6.45.

**Synthesis of Complex [(TPP)La(PPh$_2$O)$_3$Sn] (2).** To synthesize large-size lanthanum porphyrinate halides, $LaI_3$ was initially used as the starting material, following the reported method.[28] However, double-decker complex $[(TPP)_2LaLi(thf)]_2$ was obtained unexpectedly. This prompted us to adopt an alternative approach, in which we first prepared the $[(TPP)La(BH_4)]$ precursor and then reacted it with $[L^{Sn}K]$ to get complex **2**. THF (10 mL) was added to a mixture of the $[Sn(PPh_2O)_3K]$ (0.152 g, 0.2 mmol) and $[TPPLa(BH_4)(thf)_2]$ (0.182 g, 0.2 mmol). The resulting mixture was refluxed for 8 h, after which all volatiles were removed under reduced pressure. The resulting solid was extracted with DCM and filtered. Vapor diffusion of *n*-pentane into the DCM solution afforded dark purple single crystals for X-ray diffraction analysis. Yield (based on crystals): 0.162 g (0.11 mmol), 55%. $^1$H NMR (400 MHz, $CDCl_3$): $\delta$ (ppm) = 8.87 (s, 8H, *H*-Pyrrole), 8.25 (d, 4H, *J* = 6.6 Hz, Ph (ortho)), 8.14 (br, 4H, Ph (ortho)), 7.70 (br, 8H, Ph (meta)), 7.58 (br, 4H, Ph (para)), 6.90 (t, 6H, *J* = 7.5 Hz, PPh (para)), 6.76 (t, 12H, *J* = 7.0 Hz, PPh (meta)), 6.05 (t, 12H, *J* = 9.2 Hz, PPh (ortho)). $^{13}$C{$^1$H} NMR (101 MHz, $CDCl_3$): $\delta$ (ppm) = 150.1 ($C_{ipso}$-Pyrrole), 144.6 ($C_{ipso}$-(Ph or PPh), only one could be detected), 135.1 ($C_{ortho}$-Ph), 134.9 ($C_{ortho}$-Ph), 131.2 (*C*-Pyrrole), 129.4 ($C_{para}$-PPh), 127.8 ($C_{ortho}$-PPh), 127.76 ($C_{meta}$-PPh), 126.7 ($C_{meta}$-Ph), 126.2 ($C_{meta}$-Ph), 125.7($C_{para}$-Ph), 122.8 (-C=C-C−). IR (ATR): $\tilde{\nu}$ (cm$^{-1}$) = 3049 (m), 2167 (w), 1952 (w), 1889 (w), 1803 (w), 1593 (m), 1573 (w), 1508 (w), 1468 (m), 1433 (s), 1322 (m), 1196 (w), 1177 (w), 1156 (w), 1114 (s), 1074 (w), 1061 (vs), 1025 (w), 1002 (w), 976 (s), 877 (w), 845 (w), 792 (s), 748 (m), 723 (m), 690 (s), 657 (w), 576 (w), 524 (s), 487 (m). Anal. Calcd. for $C_{80}H_{58}N_4O_3P_3SnLa$ (1473.91 g/mol): C, 65.19; H, 3.97; N, 3.80. Found: C, 65.49; H, 3.80; N, 3.76.

### Accession Codes

Deposition Numbers 2386030−2386037 contain the supplementary crystallographic data for this paper. These data can be obtained free of charge via the joint Cambridge Crystallographic Data Centre (CCDC) and Fachinformationszentrum Karlsruhe Access Structures service.

## AUTHOR INFORMATION


### Corresponding Author

**Peter W. Roesky** − *Institute of Inorganic Chemistry (AOC), Karlsruhe Institute of Technology (KIT), Karlsruhe 76131, Germany; Institute of Nanotechnology (INT), Karlsruhe Institute of Technology (KIT), Eggenstein-Leopoldshafen D-76344, Germany;* orcid.org/0000-0002-0915-3893; Email: roesky@kit.edu

### Authors

**Da Jin** − *Institute of Inorganic Chemistry (AOC), Karlsruhe Institute of Technology (KIT), Karlsruhe 76131, Germany*

**Cedric Uhlmann** − *Institute of Inorganic Chemistry (AOC), Karlsruhe Institute of Technology (KIT), Karlsruhe 76131, Germany*

**Erik K. Schneider** − *Institute of Physical Chemistry (IPC), Karlsruhe Institute of Technology (KIT), Karlsruhe D-76131, Germany*

**Tim Seifert** − *Institute of Inorganic Chemistry (AOC), Karlsruhe Institute of Technology (KIT), Karlsruhe 76131, Germany*

**Dominik Graf** − *Institute of Physical Chemistry (IPC), Karlsruhe Institute of Technology (KIT), Karlsruhe D-76131, Germany; Institute of Nanotechnology (INT), Karlsruhe Institute of Technology (KIT), Eggenstein-Leopoldshafen D-76344, Germany*

**Sergei Lebedkin** − *Institute of Nanotechnology (INT), Karlsruhe Institute of Technology (KIT), Eggenstein-Leopoldshafen D-76344, Germany*

**Patrick Weis** − *Institute of Physical Chemistry (IPC), Karlsruhe Institute of Technology (KIT), Karlsruhe D-76131, Germany;* orcid.org/0000-0001-7006-6759

**Manfred M. Kappes** − *Institute of Physical Chemistry (IPC), Karlsruhe Institute of Technology (KIT), Karlsruhe D-76131, Germany; Institute of Nanotechnology (INT), Karlsruhe Institute of Technology (KIT), Eggenstein-Leopoldshafen D-76344, Germany;* orcid.org/0000-0002-1199-1730


### Author Contributions

#D.J. and C.U. contributed equally to this work.

### Author Contributions

The manuscript was written through contributions of all authors. All authors have given approval to the final version of the manuscript.

### Notes

The authors declare no competing financial interest.
No uncommon hazards are noted.

## ACKNOWLEDGMENTS


D.J. thanks the China Scholarship Council (No. 201906030178) for the generous support. The authors gratefully acknowledge support from the Deutsche Forschungsgemeinschaft (DFG, German Research Foundation) through the Collaborative Research Centre "4f for Future" (CRC 1573 project number 471424360, projects A2 and C1).


## REFERENCES


(1) Eliseeva, S. V.; Bünzli, J.-C. G. Rare earths: jewels for functional materials of the future. *New J. Chem.* **2011**, *35*, 1165−1176.

(2) Bünzli, J.-C. G.; Eliseeva, S. V. Lanthanide NIR luminescence for telecommunications, bioanalyses and solar energy conversion. *J. Rare Earths* **2010**, *28*, 824−842.

(3) Bulach, V.; Sguerra, F.; Hosseini, M. W. Porphyrin lanthanide complexes for NIR emission. *Coord. Chem. Rev.* **2012**, *256*, 1468−1478.
(4) Mason, S. Mechanisms for f-f transition probabilities in lanthanide coordination compounds. *Inorg. Chim. Acta* **1984**, *94*, 88.
(5) De Sa, G.; Malta, O.; de Mello Donegá, C.; Simas, A.; Longo, R.; Santa-Cruz, P.; da Silva, E., Jr. Spectroscopic properties and design of highly luminescent lanthanide coordination complexes. *Coord. Chem. Rev.* **2000**, *196*, 165−195.
(6) Armelao, L.; Quici, S.; Barigelletti, F.; Accorsi, G.; Bottaro, G.; Cavazzini, M.; Tondello, E. Design of luminescent lanthanide complexes: From molecules to highly efficient photo-emitting materials. *Coord. Chem. Rev.* **2010**, *254*, 487−505.
(7) Uh, H.; Petoud, S. Novel antennae for the sensitization of near infrared luminescent lanthanide cations. *C. R. Chim.* **2010**, *13*, 668−680.
(8) Gao, W.-Y.; Chrzanowski, M.; Ma, S. Metal−metalloporphyrin frameworks: a resurging class of functional materials. *Chem. Soc. Rev.* **2014**, *43*, 5841−5866.
(9) Beletskaya, I.; Tyurin, V. S.; Tsivadze, A. Y.; Guilard, R.; Stern, C. Supramolecular chemistry of metalloporphyrins. *Chem. Rev.* **2009**, *109*, 1659−1713.
(10) Segade, A.; Castella, M.; López-Calahorra, F.; Velasco, D. Synthesis and characterization of unsymmetrically $\beta$-substituted porphyrin liquid crystals: Influence of the chemical structure on the mesophase ordering. *Chem. Mater.* **2005**, *17*, 5366−5374.
(11) Kimura, M.; Wada, K.; Ohta, K.; Hanabusa, K.; Shirai, H.; Kobayashi, N. Organic−Inorganic Composites Comprised of Ordered Stacks of Amphiphilic Molecular Disks. *J. Am. Chem. Soc.* **2001**, *123*, 2438−2439.
(12) Pasternack, R. F.; Schaefer, K. F.; Hambright, P. Resonance light-scattering studies of porphyrin diacid aggregates. *Inorg. Chem.* **1994**, *33*, 2062−2065.
(13) Gandini, S. C.; Yushmanov, V. E.; Tabak, M. Interaction of Fe(III)- and Zn(II)-tetra(4-sulfonatophenyl) porphyrins with ionic and nonionic surfactants: aggregation and binding. *J. Inorg. Biochem.* **2001**, *85*, 263−277.
(14) Yushmanov, V. E.; Imasato, H.; Tominaga, T. T.; Tabak, M. $^1$H NMR and electronic absorption spectroscopy of paramagnetic water-soluble meso-tetraarylsubstituted cationic and anionic metalloporphyrins. *J. Inorg. Biochem.* **1996**, *61*, 233−250.
(15) Hayes, L. A.; Chappell, A. M.; Jellen, E. E.; Ryzhov, V. Binding of metalloporphyrins to model nitrogen bases: Collision-induced dissociation and ion−molecule reaction studies. *Int. J. Mass spectrom.* **2003**, *227*, 111−120.
(16) Chiavarino, B.; Crestoni, M. E.; Fornarini, S.; Rovira, C. Unravelling the intrinsic features of NO binding to iron(II)- and iron(III)-hemes. *Inorg. Chem.* **2008**, *47*, 7792−7801.
(17) Karpuschkin, T.; Kappes, M. M.; Hampe, O. Binding of $O_2$ and CO to metal porphyrin anions in the gas phase. *Angew. Chem., Int. Ed.* **2013**, *52*, 10374−10377.
(18) Milne, B. F.; Kjær, C.; Houmøller, J.; Stockett, M. H.; Toker, Y.; Rubio, A.; Nielsen, S. B. On the exciton coupling between two chlorophyll pigments in the absence of a protein environment: Intrinsic effects revealed by theory and experiment. *Angew. Chem., Int. Ed.* **2016**, *55*, 6248−6251.
(19) Schissler, C.; Schneider, E. K.; Rotter, M.; Notter, S.; Geier, C.; Weis, P.; Kappes, M. M.; Bräse, S. Marriage of an N-Fused and a Regular Porphyrin in a Cofacial Ligand System. *Organometallics* **2023**, *42*, 1882−1889.
(20) Jäger, P.; Brendle, K.; Schneider, E.; Kohaut, S.; Armbruster, M. K.; Fink, K.; Weis, P.; Kappes, M. M. Photodissociation of Free Metalloporphyrin Dimer Multianions. *J. Phys. Chem. A* **2018**, *122*, 2974−2982.
(21) Jäger, P.; Brendle, K.; Schwarz, U.; Himmelsbach, M.; Armbruster, M. K.; Fink, K.; Weis, P.; Kappes, M. M. Q and Soret band photoexcitation of isolated palladium porphyrin tetraanions leads to delayed emission of nonthermal electrons over microsecond time scales. *J. Phys. Chem. Lett.* **2016**, *7*, 1167−1172.
(22) Horrocks, W. D., Jr; Wong, C.-P. Lanthanide porphyrin complexes. Evaluation of nuclear magnetic resonance dipolar probe and shift reagent capabilities. *J. Am. Chem. Soc.* **1976**, *98*, 7157−7162.
(23) Gaiduk, M.; Grigoryants, V.; Mironov, A.; Rumyantseva, V.; Chissov, V.; Sukhin, G. Fibre-laser IR luminescence diagnostics of malignant tumours using rare earth porphyrins. *J. Photochem. Photobiol. B, Biol.* **1990**, *7*, 15−20.
(24) Gao, F.; Yao, M.-X.; Li, Y.-Y.; Li, Y.-Z.; Song, Y.; Zuo, J.-L. Syntheses, structures, and magnetic properties of seven-coordinate lanthanide porphyrinate or phthalocyaninate complexes with Kläui's tripodal ligand. *Inorg. Chem.* **2013**, *52*, 6407−6416.
(25) Tanaka, D.; Inose, T.; Tanaka, H.; Lee, S.; Ishikawa, N.; Ogawa, T. Proton-induced switching of the single molecule magnetic properties of a porphyrin based $Tb^{III}$ double-decker complex. *Chem. Commun.* **2012**, *48*, 7796−7798.
(26) Wong, C.-P.; Venteicher, R. F.; Horrocks, W. D., Jr Lanthanide porphyrin complexes. Potential new class of nuclear magnetic resonance dipolar probe. *J. Am. Chem. Soc.* **1974**, *96*, 7149−7150.
(27) Foley, T. J.; Abboud, K. A.; Boncella, J. M. Synthesis of Ln(III) chloride tetraphenylporphyrin complexes. *Inorg. Chem.* **2002**, *41*, 1704−1706.
(28) Foley, T. J.; Harrison, B. S.; Knefely, A. S.; Abboud, K. A.; Reynolds, J. R.; Schanze, K. S.; Boncella, J. M. Facile preparation and photophysics of near-infrared luminescent lanthanide(III) monoporphyrinate complexes. *Inorg. Chem.* **2003**, *42*, 5023−5032.
(29) Santria, A.; Fuyuhiro, A.; Fukuda, T.; Ishikawa, N. Synthesis of a series of heavy lanthanide(III) monoporphyrinato complexes with tetragonal symmetry. *Inorg. Chem.* **2017**, *56*, 10625−10632.
(30) Wong, C. P.; Bisset, G. [5,10,15,20-Tetraphenylporphyrinato $(2^-)$] Lanthanides and Some [5,10,15,20-Tetraphenylporphyrinato $(2^-)$] Actinides. *Inorg. Synth.* **1984**, *22*, 156−162.
(31) Buchler, J. W.; De Cian, A.; Fischer, J.; Kihn-Botulinski, M.; Paulus, H.; Weiss, R. Cerium(IV) bis(octaethylporphyrinate) and dicerium(III) tris(octaethylporphyrinate): Parents of a new family of lanthanoid double-decker and triple-decker molecules. *J. Am. Chem. Soc.* **1986**, *108*, 3652−3659.
(32) He, H.; Wong, W.-K.; Guo, J.; Li, K.-F.; Wong, W.-Y.; Lo, W.-K.; Cheah, K.-W. Monoporphyrinate neodymium(III) complexes stabilized by tripodal ligand: synthesis, characterization and luminescence. *Inorg. Chim. Acta* **2004**, *357*, 4379−4388.
(33) Wong, W.-K.; Hou, A.; Guo, J.; He, H.; Zhang, L.; Wong, W.-Y.; Li, K.-F.; Cheah, K.-W.; Xue, F.; Mak, T. C. Synthesis, structure and near-infrared luminescence of neutral 3d−4f bi-metallic monoporphyrinate complexes. *J. Chem. Soc., Dalton Trans.* **2001**, 3092−3098.
(34) Hu, J.-Y.; Ning, Y.; Meng, Y.-S.; Zhang, J.; Wu, Z.-Y.; Gao, S.; Zhang, J.-L. Highly near-IR emissive ytterbium(III) complexes with unprecedented quantum yields. *Chem. Sci.* **2017**, *8*, 2702−2709.
(35) Zhu, X.; Wang, P.; Leung, H. W. C.; Wong, W.; Wong, W.; Kwong, D. W. J. Synthesis, Characterization, and DNA-Binding and -Photocleavage Properties of Water-Soluble Lanthanide Porphyrinate Complexes. *Chem. − Eur. J.* **2011**, *17*, 7041−7052.
(36) He, H.; Guo, J.; Zhao, Z.; Wong, W. K.; Wong, W. Y.; Lo, W. K.; Li, K. F.; Luo, L.; Cheah, K. W. Synthesis, Characterization and Near-Infrared Photoluminescence of Monoporphyrinate Lanthanide Complexes Containing an Anionic Tripodal Ligand. *Eur. J. Inorg. Chem.* **2004**, *9*, 837−845.
(37) He, H.; He, G.; Ng, S. W. [Hydridotris(pyrazol-1-yl)borato-$\kappa^3$N,N',N"][5,10,15,20-tetrakis(4-methylphenyl)porphyrinato-$\kappa^4$N,N',N"N'"] samarium(III) toluene 1.75-solvate. *Acta Crystallogr. Sect. Sect. E: Struct. Rep. Online* **2007**, *63*, No. m2878.
(38) Rong, W.; Liu, D.; Zuo, H.; Pan, Y.; Jian, Z.; Li, S.; Cui, D. Rare-earth-metal complexes bearing phosphazene ancillary ligands: structures and catalysis toward highly trans-1,4-selective (Co)-polymerizations of conjugated dienes. *Organometallics* **2013**, *32*, 1166−1175.
(39) Ivanova, I.; Ilyukhin, A.; Pyatova, E.; Demin, S.; Zhogin, E.; Tsebrikova, G.; Solov'ev, V.; Baulin, D.; Baulin, V.; Tsivadze, A. Y. Effect of the [2-(diphenylphosphorylmethoxy) phenyl] diphenylphos-

phine oxide derivative structures on the extraction and ion-selective properties toward rare-earth elements. *Russ. Chem. Bull.* **2020**, *69*, 1336−1343.
(40) Guo, F.; Nishiura, M.; Li, Y.; Hou, Z. Copolymerization of Isoprene and Nonconjugated $\alpha$, $\omega$-Dienes by Half-Sandwich Scandium Catalysts with and without a Coordinative Side Arm. *Chem-Asian J.* **2013**, *8*, 2471−2482.
(41) Yu, X.; Marks, T. J. Organophosphine oxide/sulfide-substituted lanthanide binaphtholate catalysts for enantioselective hydroamination/cyclization. *Organometallics* **2007**, *26*, 365−376.
(42) Tolpygin, A. O.; Glukhova, T. A.; Cherkasov, A. V.; Fukin, G. K.; Aleksanyan, D. V.; Cui, D.; Trifonov, A. A. Bis(alkyl) rare-earth complexes supported by a new tridentate amidinate ligand with a pendant diphenylphosphine oxide group. Synthesis, structures and catalytic activity in isoprene polymerization. *Dalton Trans.* **2015**, *44*, 16465−16474.
(43) Berny, F.; Muzet, N.; Troxler, L.; Dedieu, A.; Wipff, G. Interaction of $M^{3+}$ lanthanide cations with amide, pyridine, and phosphoryl O=$PPh_3$ ligands: a quantum mechanics study. *Inorg. Chem.* **1999**, *38*, 1244−1252.
(44) Chesnut, D. An ab initio nuclear magnetic resonance and atoms-in-molecules study of the PO bond in phosphine oxides. *J. Am. Chem. Soc.* **1998**, *120*, 10504−10510.
(45) Platt, A. W. Lanthanide phosphine oxide complexes. *Coord. Chem. Rev.* **2017**, *340*, 62−78.
(46) Jin, D. *Coordination Chemistry of Formazanates and Small Molecule Activation of Silylenes*; Cuvillier Verlag: 2023.
(47) Uhlmann, C., Synthese von Lanthanoid Multideckerkomplexen mit heterozyklischen Liganden sowie Lanthanoidkomplexen auf Basis eines tripodalen Zinnliganden. https://publikationen.bibliothek.kit.edu/1000171903.
(48) Härling, S. M.; Krieck, S.; Görls, H.; Westerhausen, M. Influence of 18-Crown-6 Ether Coordination on the Catalytic Activity of Potassium and Calcium Diarylphosphinites in Hydrophosphorylation Reactions. *Inorg. Chem.* **2017**, *56*, 9255−9263.
(49) Allen, F. H.; Kennard, O.; Watson, D. G.; Brammer, L.; Orpen, A. G.; Taylor, R. Tables of bond lengths determined by X-ray and neutron diffraction. Part 1. Bond lengths in organic compounds. *J. Chem. Soc., Perkin Trans.* **1987**, S1−S19.
(50) Starzewski, K. H. O.; Pregosin, P. S.; Rüegger, H. $^{31}$P-, $^{119}$Sn- and $^{195}$Pt- NMR. Studies of Trichlorostannate Complexes of Pt(II) and Pd(II). $^{2}J(^{119}Sn, ^{117}Sn)$- Values. *Helv. Chim. Acta* **1982**, *65*, 785−797.
(51) Kläui, W.; Mocigemba, N.; Weber-Schuster, A.; Bell, R.; Frank, W.; Mootz, D.; Poll, W.; Wunderlich, H. $[(C_5H_5)Co\{P(O)(OH)_2\}_3H]$: A Novel Organometallic Tris-phosphonic Acid That Dissolves Glass to Form a Six-Coordinate Silicon Complex. *Chem. − Eur. J.* **2002**, *8*, 2335−2340.
(52) Kläui, W. The coordination chemistry and organometallic chemistry of tridentate oxygen ligands with $\pi$-donor properties. *Angew. Chem., Int. Ed.* **1990**, *29*, 627−637.
(53) Kläui, W. $[(C_5H_5)Co\{P(O)(OC_2H_5)_2\}_3]^-$: Eine einfache Synthese eines metallorganischen Tripodliganden und seine Reaktivität gegenüber den Kationen der III. Hauptgruppe/$[(C_5H_5)Co\{P(O)(OC_2H_5)_2\}_3]^-$: A Convenient Synthesis of an Organometallic Tripod Ligand and its Reactivity towards the Main Group III Cations. *Z. Naturforsch. B* **1979**, *34*, 1403−1407.
(54) Arnold, J.; Dawson, D. Y.; Hoffman, C. G. Synthesis and characterization of lithium, sodium, and potassium porphyrin complexes. X-ray crystal structures of $Li_2(C_6H_{12}O_2)_2$TMPP, $Na_2(THF)_4$OEP, and $K_2$(pyridine)$_4$OEP. *J. Am. Chem. Soc.* **1993**, *115*, 2707−2713.
(55) Cendrowski-Guillaume, S. M.; Nierlich, M.; Lance, M.; Ephritikhine, M. First chemical transformations of lanthanide borohydride compounds: synthesis and crystal structures of $[(\eta\text{-}C_8H_8)Nd(BH_4)(THF)]_2$ and $[(\eta\text{-}C_8H_8)Nd(THF)_4][BPh_4]$. *Organometallics* **1998**, *17*, 786−788.
(56) Münzfeld, L.; Hauser, A.; Gamer, M. T.; Roesky, P. W. Monocyclononatetraenyl lanthanide complexes. *Chem. Commun.* **2023**, *59*, 9070−9073.
(57) Sues, P. E.; Lough, A. J.; Morris, R. H. Synthesis, Characterization, and Activity of Yttrium(III) Nitrate Complexes Bearing Tripodal Phosphine Oxide and Mixed Phosphine−Phosphine Oxide Ligands. *Inorg. Chem.* **2012**, *51*, 9322−9332.
(58) Llunell, M.; Alemany, P.; Alvarez, S., *Shape 2.1 for Windows (32 bit)*.
(59) Santria, A.; Fuyuhiro, A.; Fukuda, T.; Ishikawa, N. Determination of ligand field splitting in lanthanide(III) monoporphyrinato complexes. *Dalton Trans.* **2019**, *48*, 7685−7692.
(60) Mandal, A. K.; Taniguchi, M.; Diers, J. R.; Niedzwiedzki, D. M.; Kirmaier, C.; Lindsey, J. S.; Bocian, D. F.; Holten, D. Photophysical properties and electronic structure of porphyrins bearing zero to four meso-phenyl substituents: New insights into seemingly well understood tetrapyrroles. *J. Phys. Chem. A* **2016**, *120*, 9719−9731.
(61) Horváth, O.; Huszánk, R.; Valicsek, Z.; Lendvay, G. Photophysics and photochemistry of kinetically labile, water-soluble porphyrin complexes. *Coord. Chem. Rev.* **2006**, *250*, 1792−1803.
(62) Schissler, C.; Schneider, E. K.; Lebedkin, S.; Weis, P.; Niedner-Schatteburg, G.; Kappes, M. M.; Bräse, S. Novel Cofacial Porphyrin-Based Homo- and Heterotrimetallic Complexes of Transition Metals. *Chem. − Eur. J.* **2021**, *27*, 15202−15208.
(63) Crouch, A. M.; Langford, C. H. Photophysical behaviour of zinc tetraphenylporphyrins in solutions and polymer films. *J. Photochem. Photobiol., A* **1990**, *52*, 55−64.
(64) Magdaong, N. C. M.; Taniguchi, M.; Diers, J. R.; Niedzwiedzki, D. M.; Kirmaier, C.; Lindsey, J. S.; Bocian, D. F.; Holten, D. Photophysical properties and electronic structure of zinc(II) porphyrins bearing 0−4 meso-phenyl substituents: zinc porphine to zinc tetraphenylporphyrin (ZnTPP). *J. Phys. Chem. A* **2020**, *124*, 7776−7794.
(65) Gouterman, M.; Schumaker, C. D.; Srivastava, T.; Yonetani, T. Absorption and luminescence of yttrium and lanthanide octaethylporphin complexes. *Chem. Phys. Lett.* **1976**, *40*, 456−461.
(66) Kaizu, Y.; Asano, M.; Kobayashi, H. Dual fluorescence from two erbium(III) porphyrins. *J. Phys. Chem.* **1986**, *90*, 3906−3910.
(67) Harriman, A. Luminescence of porphyrins and metalloporphyrins. Part 1.—Zinc(II), nickel(II) and manganese(II) porphyrins. *J. Chem. Soc., Faraday Trans. 1* **1980**, *76*, 1978−1985.
(68) Khalil, G. E.; Thompson, E. K.; Gouterman, M.; Callis, J. B.; Dalton, L. R.; Turro, N. J.; Jockusch, S. NIR luminescence of gadolinium porphyrin complexes. *Chem. Phys. Lett.* **2007**, *435*, 45−49.